Computers and Concrete, *Vol. 21, No. 5 (2018) 569-582*
DOI: https://doi.org/10.12989/cac.2018.21.5.569

Vibration and instability of nanocomposite pipes conveying fluid mixed by nanoparticles resting on viscoelastic foundation

Abolfazl Jafari Natanzi, Gholamreza Soleimani Jafari* and Reza Kolahchi

Department of Mechanical Engineering, Kashan Branch, Islamic Azad University, Kashan, Iran

(Received October 25, 2017, Revised January 26, 2018, Accepted January 29, 2018)

Abstract. In this study, nonlinear vibration and stability of a polymeric pipe reinforced by single-walled carbon naotubes (SWCNTs) conveying fluid-nanoparticles mixture flow is investigated. The Characteristics of the equivalent composite are determined using Mori-Tanaka model considering agglomeration effects. The surrounding elastic medium is simulated by orthotropic visco-Pasternak medium. Employing nonlinear strains-displacements, stress-strain energy method the governing equations were derived using Hamilton's principal. Differential quadrature method (DQM) is used for obtaining the frequency and critical fluid velocity. The influence of volume percent of SWCNTs, agglomeration, geometrical parameters of pipe, viscoelastic foundation and fluid velocity are shown on the frequency and critical fluid velocity of pipe. Results showed the increasing volume percent of SWCNTs leads to higher frequency and critical fluid velocity.

Keywords: pipe; stability; SWCNT; agglomeration; fluid-nanoparticles mixture

1. Introduction

Composite cylindrical shell constructs are more widely used than the other geometric shapes in the industries due to the desired ratio of the strength to the weight and easy manufacturing. As these constructs are used, different dynamic energies effect on them which consequently may influence on their performance or that of in-made equipment.

Love (1892) was the first researchers proposed the thin shell theory based on the linear elasticity theory. Following him, some other researchers such as Donnell (1934), Sanders (1959), Flog *et al*. (1973) applied the other hypothesis on the linear elasticity theory and proposed some more accurate movement equations. A geometrically nonlinear wind-induced vibration analysis strategy for large-span single-layer reticulated shell structures based on the nonlinear finite element method was introduced by Li and Tamura (2005). Amabili (2008) compared the different theories to analyze the nonlinear vibrations of layer cylindrical shells in a comprehensive study. The vibrations of sandwich cylindrical shapes shells were analyzed by Kumar *et al*. (2013) based on Zigzag shear theory. Kamarian *et al*. (2014) studied functionally graded sandwich cylindrical shells in the elastic area. Functionally graded cylindrical shells were analyzed by Mantari and Guedes Soares (2014) using high order sine shear theory in which system governing equations are obtained using the method of energy and virtual work principle. Duc and Than (2015) studied the dynamic and the vibrations of the functionally graded cylindrical shells. Sofiyev (2016) studied nonlinear vibrations of the functionally graded cylindrical shells using the orthotropic shear theory. Bahadori and Najafizadeh (2015) analyzed the free vibrations of the functionally graded cylindrical shells in the elastic area.

Cylindrical shells with fluid are widely used in the industry and biomechanical systems. For example, the thermal shields of the nuclear reactors and the ignition motor of the airplanes, thermal convertors, oil and gas transportation pipes, veins, pulmonary system and etc are modeled by the cylindrical shells having fluid. Amabili (2003) has mostly analyzed and studied these shells. The effect of the shell fluid is studied by Paidoussis and Denise (1972), Weaver and Unny (1973), Paidoussis *et al.* (2003, 1985), Amabili and Garziera (2002). The pressure caused by the fluid is extracted by the function of confusion potential caused by the axial velocity of the fluid in the shell. The effect of the geometric parameters on the nonlinear vibrations in the cylindrical shell with fluid is studied by Pellicanoa *et al.* (2002). De Bellis *et al.* (2010) analyzed the dynamic stability of the fluid carrying tube in the elasticity area. They used Timoshenko beam model to mathematically model the construct and used Galerkin method to analyze the system. This article mainly discusses the critical velocity of the fluid and analyzes its different parameters. Wang (2009) analyzed the nonlinear dynamic of the tube with variable fluid. Numerical analysis of a rotating cylindrical shell with fluid was performed by Bochkarev and Matveenko (2013). Dai *et al.* (2014) studied fluid carrying tubes using Euler- Bernoulli beam theory, considering the effect of the fluid damping and eddy current caused in the tube. Ghorbanpour Arani *et al.* (2016) analyzed the vibrations and instabilities in the Nano composite cylindrical shell surrounded by tow piezoelectric layers.

*Corresponding author, Ph.D.
E-mail: soleimani.kashan@gmail.com

http://www.techno-press.org/?journal=cac&subpage=8
ISSN: 1598-8198 (Print), 1598-818X (Online)

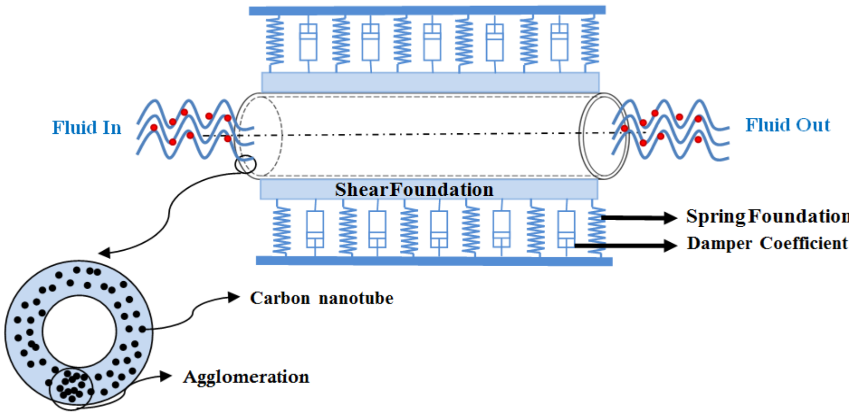

Fig. 1 Scheme of nano composite tube with nanoparticles mixed fluid considering the effect of accumulation

Mechanical analysis of nanostructures, sensor and compter programs has been reported by many researchers (Zemri 2015, Larbi Chaht 2015, Belkorissat 2015, Ahouel 2016, Bounouara 2016, Bouafia 2017, Besseghier 2017, Bellifa 2017, Mouffoki 2017, Khetir 2017, Yang and Yu 2017, Li *et al*. 2017, Padhy and Panda 2017, Zhao *et al*. 2017, Rishikeshan and Ramesh 2017, Wen *et al*. 2017, Torres-Jimenez and Rodriguez-Cristerna 2017, Liu *et al*. 2018). There is non- composite structure in all of the above mentioned works. These structures, particularly polymeric Nano composites are widely used in the industries such as in the sensors and operators of the oil and gas transportation pipes. As the technology is advancing, these structures have found a special position in the industries and they are increasingly used because the static and dynamic behavior of the construct can be improved by the good mechanical and thermal features of the carbon Nano tubes as the reinforcers. A few works have done in this regard. Messina and Soldatos (1999) studied the free vibrations of the composite cylindrical shell. Tan and Tong (2001) proposed a micromechanical model to calculate the composite equivalent properties. The free vibrations of the composite cylindrical shell with fluid were studied by Kadoli and Ganesan (2003). The dynamic behavior of the fluid carrying composite cylindrical shell was considered by Seo *et al.* (2015). Wuite and Adali (2005) analyzed the tension in the beams reinforced by the carbon Nano tubes and used Mori-Tanaka Model to equalize the composite equivalent properties. Liew *et al.* (2014) analyzed the post buckling of the Nano composite shells. Mixing law was used in this research to gain Nano composite equivalent properties. In another similar work, Lei *et al.* (2014) analyzed the dynamic stability of the panels reinforced by carbon Nano tubes.

So, it is concluded that many researchers have been performed to analyze the vibrations and instability of the cylindrical shells with fluid so far but no studies have been done about Nano composite shells with the Nano particle fluid in spite of being modern. So, the different aspects between the present research and the other ones are as composite shell (Using carbon Nano tubes as reinforcement phase), considering the accumulation of the Nano tubes, passage of the fluid with Nano particles through the shell and considering the viscoelastic area around the tube. Some explanations will be given briefly about the Nano composites and the methods of producing the composite equivalent properties in the following due to this fact that the background material of the shell is made of polymer and reinforced by the carbon Nano tubes.

2. Mathematical modeling

Fig. 1 shows a tube modeled by a circular cylindrical shell with the mean radius of R, thickness of h , length of L, density of ρ and the cylindrical coordinate system of ($x,\theta,\rho=R+z$). This shell is reinforced by the carbon nanotubes and has a fluid mixed with the nanoparticles. The viscoelastic area around the tube is modeled by the Winkler vertical coefficient k_w, shear coefficient k_g and the Damper coefficient c_d .

There are many new theories for modeling of different structures. Some of the new theories have been used by Tounsi and co-authors (Bessaim 2013, Bouderba 2013, Belabed 2014, Ait Amar Meziane 2014, Zidi 2014, Hamidi 2015, Bourada 2015, Bousahla *et al.* 2016a, b, Beldjelili 2016, Boukhari 2016, Draiche 2016, Bellifa 2015, Attia 2015, Mahi 2015, Ait Yahia 2015, Bennoun 2016, El-Haina 2017, Menasria 2017, Chikh 2017). In this paper, classical theory is used. Movement field can be expressed as below based on the classic theory (Reddy 2004)

$$u_1(x,\theta,z,t)=u(x,\theta,t)-z\frac{\partial w(x,\theta,t)}{\partial x}, \tag{1}$$

$$u_2(x,\theta,z,t)=v(x,\theta,t)-\frac{z}{R}\frac{\partial w(x,\theta,t)}{\partial \theta}, \tag{2}$$

$$u_3(x,\theta,z,t)=w(x,\theta,t), \tag{3}$$

in which (u,v,w) are the movement elements of the middle plane (z=0) in the length of the axes (x,θ,z). The relationships of strain-displacement are

$$\varepsilon_{xx}=\frac{\partial u}{\partial x}-z\frac{\partial^2 w}{\partial x^2}, \tag{4}$$

$$\varepsilon_{\theta\theta}=\frac{\partial v}{R\partial \theta}+\frac{w}{R}-\frac{z}{R^2}\frac{\partial^2 w}{\partial \theta^2}, \tag{5}$$

$$\varepsilon_{xy}=\frac{1}{2}\left(\frac{\partial u}{R\partial\theta}+\frac{\partial v}{\partial x}\right)-z\frac{\partial^2 w}{R\partial x\partial\theta}, \tag{6}$$

The construct's strain -tension relationships are simplified as

$$\begin{bmatrix}\sigma_{xx}\\ \sigma_{\theta\theta}\\ \tau_{x\theta}\end{bmatrix}=\begin{bmatrix}C_{11} & C_{12} & 0\\ C_{21} & C_{22} & 0\\ 0 & 0 & C_{66}\end{bmatrix}\begin{bmatrix}\varepsilon_{xx}\\ \varepsilon_{\theta\theta}\\ \gamma_{x\theta}\end{bmatrix}, \tag{7}$$

The potential energy of the Nano composite tube is as the following

$$U=\int_V\left(\sigma_{xx}\varepsilon_{xx}+\sigma_{\theta\theta}\varepsilon_{\theta\theta}+\sigma_{x\theta}\gamma_{x\theta}\right)dV, \tag{8}$$

By replacing the strain- shift equations in the above relationships, we have

$$\begin{aligned}U=\int_{-\frac{h}{2}}^{\frac{h}{2}}\int_A\Bigg(&\sigma_x\left(\frac{\partial u}{\partial x}+0.5\left(\frac{\partial w}{\partial x}\right)^2-z\frac{\partial^2 w}{\partial x^2}\right)\\ &+\sigma_\theta\left(\frac{\partial v}{R\partial\theta}+\frac{w}{R}+0.5\left(\frac{\partial w}{R\partial\theta}\right)^2\right.\\ &\left.-z\frac{\partial^2 w}{R^2\partial\theta^2}\right)+\sigma_{x\theta}\left(\frac{\partial u}{R\partial\theta}+\frac{\partial v}{\partial x}+\frac{\partial w}{R\partial\theta}\frac{\partial w}{\partial x}-2z\frac{\partial^2 w}{R\partial\theta\partial x}\right)\Bigg)dz\,dA\end{aligned} \tag{9}$$

By defining the energy and intra -plane moments as below

$$\begin{Bmatrix}N_x\\ N_\theta\\ N_{x\theta}\end{Bmatrix}=\int_{-\frac{h}{2}}^{\frac{h}{2}}\begin{Bmatrix}\sigma_x\\ \sigma_\theta\\ \tau_{x\theta}\end{Bmatrix}dz, \tag{10}$$

$$\begin{Bmatrix}M_x\\ M_\theta\\ M_{x\theta}\end{Bmatrix}=\int_{-\frac{h}{2}}^{\frac{h}{2}}\begin{Bmatrix}\sigma_x\\ \sigma_\theta\\ \tau_{x\theta}\end{Bmatrix}zdz, \tag{11}$$

relationship (9) will be as

$$\begin{aligned}U=\int_A\Bigg(&N_x\left(\frac{\partial u}{\partial x}+0.5\left(\frac{\partial w}{\partial x}\right)^2\right)-M_x\frac{\partial^2 w}{\partial x^2}\\ &+N_\theta\left(\frac{\partial v}{R\partial\theta}+\frac{w}{R}+0.5\left(\frac{\partial w}{R\partial\theta}\right)^2\right)\\ &-M_\theta\frac{\partial^2 w}{R^2\partial\theta^2}+N_{x\theta}\left(\frac{\partial u}{R\partial\theta}+\frac{\partial v}{\partial x}+\frac{\partial w}{R\partial\theta}\frac{\partial w}{\partial x}\right)\\ &-2M_{x\theta}\frac{\partial^2 w}{R\partial\theta\partial x}\Bigg)dA\end{aligned} \tag{12}$$

Kinetic energy of the construct is as

$$K=\frac{\rho}{2}\int_v\left((\frac{\partial u_1}{\partial t})^2+(\frac{\partial u_2}{\partial t})^2+(\frac{\partial u_3}{\partial t})^2\right)dV, \tag{13}$$

where ρ is the nano composite shell equivalent density. By replacing the movement fields in the above equation, we will have

$$\begin{aligned}K=\frac{\rho}{2}\int_{-\frac{h}{2}}^{\frac{h}{2}}\int_A\Bigg[&(\frac{\partial u}{\partial t})^2-2z\frac{\partial u}{\partial t}\frac{\partial^2 w}{\partial t\partial x}\\ &+z^2\left(\frac{\partial^2 u}{\partial t\partial x}\right)^2+(\frac{\partial v}{\partial t})^2-2z\frac{\partial v}{\partial t}\frac{\partial^2 w}{\partial t\partial\theta}\\ &+z^2\left(\frac{\partial^2 w}{\partial t\partial\theta}\right)^2+(\frac{\partial w}{\partial t})^2\Bigg]dzdA\end{aligned} \tag{14}$$

By integration in the thickness direction and considering this fact that the range of integer is symmetric, the odd integers will be zero. So the kinetic energy would be simplified as below:

$$\begin{aligned}K=\int\Bigg(&\frac{\rho}{2}\left(\frac{h^3}{12}\left((\frac{\partial^2 u}{\partial t\,\partial x})^2+(\frac{\partial^2 w}{\partial t\partial\theta})^2\right)\right)\\ &+h\left((\frac{\partial u}{\partial t})^2+(\frac{\partial v}{\partial t})^2+(\frac{\partial w}{\partial t})^2\right)\Bigg)dA.\end{aligned} \tag{15}$$

The work of the external energies is divided to two parts: work of the viscoelastic area around the tube and work of the fluid in the tube.

→ Work of the Viscoelastic Area

Viscoelastic area around the tube includes the spring, shear and damper coefficient whose equivalent energy is gained according to the below (Ghorbanpour Arani 2016)

$$F_{elastic}=\left(-k_w w-c_d\dot{w}+k_g\nabla^2 w\right), \tag{16}$$

in which k_w, k_g and c_d are the Winkler vertical flexibility coefficient, Pasternak shear coefficient and damper coefficient, respectively. So, the external work W_e in the viscoelastic area is

$$W_e=-\int\left(k_w w+c_d\dot{w}-k_g\nabla^2 w\right)wdA, \tag{17}$$

Considering the fluid incompressible, Newtonian and viscose, the fluid's behavior governing equation is as

$$\rho_f\frac{d\mathbf{V}}{dt}=-\nabla\mathbf{P}+\mu\nabla^2\mathbf{V}+\mathbf{F}_{body}, \tag{18}$$

which is known as Navier- Stockes in which $\mathbf{V}\equiv(v_z,v_\theta,v_x)$ is the velocity of the fluid in the cylindrical coordinates in the direction of length, circumference and radius and $\mathbf{P}$, μ and ρ_f are pressure, viscosity and the dense of the fluid, respectively and $\mathbf{F}_{body}$ is the volumetric force. The operator of the complete derivative is as below in the Navier- Stockes equation

$$\frac{d}{dt}=\frac{\partial}{\partial t}+v_x\frac{\partial}{\partial x}+v_\theta\frac{\partial}{\partial\theta}+v_z\frac{\partial}{\partial z}, \tag{19}$$

The relative velocity and acceleration are equal in the direction of the radial movement in the contact point of the fluid and tube. So

$$v_z=\frac{dw}{dt}, \tag{20}$$

Using Eqs. (19) and (20) and placing them in Eq. (18), the pressure in the tube will be

$$\frac{\partial p_z}{\partial z} = -\rho_f\left(\frac{\partial^2 w}{\partial t^2} + 2v_x\frac{\partial^2 w}{\partial x\partial t} + v_x{}^2\frac{\partial^2 w}{\partial x^2}\right) + \mu\left(\frac{\partial^3 w}{\partial x^2\partial t} + \frac{\partial^3 w}{R^2\partial\theta^2\partial t} + v_x\left(\frac{\partial^3 w}{\partial x^3} + \frac{\partial^3 w}{R^2\partial\theta^2\partial x}\right)\right), \tag{21}$$

If two sides of the equality are multiplied to the interior surface of the tube (A), the radial force in the tube is calculated

$$F_{fluid} = A\frac{\partial p_z}{\partial z} = -\rho_f\left(\frac{\partial^2 w}{\partial t^2} + 2v_x\frac{\partial^2 w}{\partial x\partial t} + v_x{}^2\frac{\partial^2 w}{\partial x^2}\right) + \mu\left(\frac{\partial^3 w}{\partial x^2\partial t} + \frac{\partial^3 w}{R^2\partial\theta^2\partial t} + v_x\left(\frac{\partial^3 w}{\partial x^3} + \frac{\partial^3 w}{R^2\partial\theta^2\partial x}\right)\right), \tag{22}$$

Finally, the external work caused by the fluid pressure is determined by

$$W_f = \int (F_{fluid})w dA = \int\left(-\rho_f\left(\frac{\partial^2 w}{\partial t^2} + 2v_x\frac{\partial^2 w}{\partial x\partial t} + v_x{}^2\frac{\partial^2 w}{\partial x^2}\right) + \mu\left(\frac{\partial^3 w}{\partial x^2\partial t} + \frac{\partial^3 w}{R^2\partial\theta^2\partial t} + v_x\left(\frac{\partial^3 w}{\partial x^3} + \frac{\partial^3 w}{R^2\partial\theta^2\partial x}\right)\right)\right) wdA, \tag{23}$$

Now, applying Hamilton principle, using fractional integral and sorting the relationships in the direction of the mechanical movements will lead to the three main equations

$$\frac{\partial N_x}{\partial x} + \frac{\partial N_{x\theta}}{R\partial\theta} = \rho h\frac{\partial^2 u}{\partial t^2}, \tag{24}$$

$$\frac{\partial N_\theta}{R\partial\theta} + \frac{\partial N_{x\theta}}{\partial x} = \rho h\frac{\partial^2 v}{\partial t^2}, \tag{25}$$

$$\frac{\partial^2 M_x}{\partial x^2} + \frac{2\partial^2 M_{x\theta}}{R\partial x\partial\theta} + \frac{\partial^2 M_\theta}{R^2\partial\theta^2} - \frac{N_\theta}{R} + N_x\frac{\partial^2 w}{\partial x^2} + N_\theta\frac{\partial^2 w}{R^2\partial\theta^2} + N_{x\theta}\frac{2\partial^2 w}{R\partial x\partial\theta} + F_{elastic} + F_{fluid} = \rho h\frac{\partial^2 w}{\partial t^2}, \tag{26}$$

By integrating Eqs. (10) and (11) in the direction of thickness and using Eq. (7), the relationships of the forces and interior moments of the tube can be calculated as

$$N_x = h\left(C_{11}\left(\frac{\partial u}{\partial x} + 0.5\left(\frac{\partial w}{\partial x}\right)^2\right) + C_{12}\left(\frac{\partial v}{R\partial\theta} + \frac{w}{R} + 0.5\left(\frac{\partial w}{R\partial\theta}\right)^2\right)\right), \tag{27}$$

$$N_\theta = h\left(C_{12}\left(\frac{\partial u}{\partial x} + 0.5\left(\frac{\partial w}{\partial x}\right)^2\right) + C_{22}\left(\frac{\partial v}{R\partial\theta} + \frac{w}{R} + 0.5\left(\frac{\partial w}{R\partial\theta}\right)^2\right)\right), \tag{28}$$

$$N_{x\theta} = h\left(C_{66}\left(\frac{\partial u}{R\partial\theta} + \frac{\partial v}{\partial x} + \frac{\partial w}{R\partial\theta}\frac{\partial w}{\partial x}\right)\right), \tag{29}$$

$$M_x = \frac{h^3}{12}\left(C_{11}\left(-z\frac{\partial^2 w}{\partial x^2}\right) + C_{12}\left(-z\frac{\partial^2 w}{R^2\partial\theta^2}\right)\right), \tag{30}$$

$$M_\theta = \frac{h^3}{12}\left(C_{12}\left(-z\frac{\partial^2 w}{\partial x^2{}_x}\right) + C_{22}\left(-z\frac{\partial^2 w}{R^2\partial\theta^2}\right)\right), \tag{31}$$

$$M_{x\theta} = \frac{h^3}{12}C_{66}\left(-2z\frac{\partial^2 w}{R\partial\theta\partial x}\right). \tag{32}$$

Now, placing the Eqs. (27) to (32) in the main equations and using the dimensionless parameters of

$$\gamma = \frac{h}{L},\quad \xi = \frac{x}{L},\quad \beta = \frac{h}{R}, \{\bar{u},\bar{v},\bar{w}\} = \frac{\{u,v,w\}}{h}, ,\bar{C}_{kij} = \frac{C_{kij}}{C_{11}},\ K_w = \frac{hk_w}{C_{11}},\quad K_g = \frac{k_g}{hC_{11}}, \bar{\rho}_k = \frac{\rho_k}{\rho_f}, \bar{\mu} = \frac{\mu}{h\sqrt{C_{11}\rho_f}},\ V_x = v_x\sqrt{\frac{\rho_f}{C_{11}}}, \bar{t} = \frac{t}{h\sqrt{\frac{\rho_f}{C_{11}}}},\ C_d = \frac{c_d}{h^2\sqrt{C_{11}\rho_f}}, \tag{33}$$

these formed relationships will be produced according to the mechanical movements

$$(\gamma^2)\left(\frac{\partial^2\bar{u}}{\partial\xi^2} + \frac{\partial\bar{w}}{\partial\xi}\frac{\partial^2\bar{w}}{\partial\xi^2}\right) + \gamma\beta\bar{C}_{12}\left(\frac{\partial^2\bar{v}}{\partial\xi\partial\theta} + \frac{\partial\bar{w}}{\partial\xi} + \beta\frac{\partial\bar{w}}{\partial\theta}\frac{\partial^2\bar{w}}{\partial\xi\partial\theta}\right) + \beta\bar{C}_{66}\left(\beta\frac{\partial^2\bar{u}}{\partial\theta^2} + \gamma\frac{\partial^2\bar{v}}{\partial\xi\partial\theta} + \beta\frac{\partial\bar{w}}{\partial\xi}\frac{\partial^2\bar{w}}{\partial\theta^2} + \gamma\frac{\partial\bar{w}}{\partial\xi} + \beta\frac{\partial\bar{w}}{\partial\theta}\frac{\partial^2\bar{w}}{\partial\xi\partial\theta}\right) = \frac{\partial^2\bar{u}}{\partial\bar{t}^2} \tag{34}$$

$$\beta\bar{C}_{12}\left(\gamma\frac{\partial^2\bar{u}}{\partial\xi\partial\theta} + \gamma^2\frac{\partial\bar{w}}{\partial\xi}\frac{\partial^2\bar{w}}{\partial\xi\partial\theta}\right) + \beta^2\bar{C}_{22}\left(\frac{\partial^2\bar{v}}{\partial\theta^2} + \frac{\partial\bar{w}}{\partial\theta} + \beta\frac{\partial\bar{w}}{\partial\theta}\frac{\partial^2\bar{w}}{\partial\theta^2}\right) + \gamma\bar{C}_{66}\left(\beta\frac{\partial^2\bar{u}}{\partial\xi\partial\theta} + \gamma\frac{\partial^2\bar{v}}{\partial\xi^2} + \beta\gamma\frac{\partial^2\bar{w}}{\partial\theta\partial\xi}\frac{\partial\bar{w}}{\partial\xi} + \beta\gamma\frac{\partial\bar{w}}{\partial\theta}\frac{\partial^2\bar{w}}{\partial\xi^2}\right) = \frac{\partial^2\bar{v}}{\partial\bar{t}^2} \tag{35}$$

$$\frac{\gamma^2}{12}\left(-\gamma^2\frac{\partial^4\bar{w}}{\partial\xi^4} - \bar{C}_{12}\beta^2\frac{\partial^4\bar{w}}{\partial\xi^2\partial\theta^2}\right) - \frac{\gamma^2\beta^2\bar{C}_{66}}{3}\left(\frac{\partial^4\bar{w}}{\partial\xi^2\partial\theta^2}\right) - \gamma\beta\bar{C}_{12}\left(\frac{\partial\bar{u}}{\partial\xi} + \frac{\gamma}{2}\left(\frac{\partial\bar{w}}{\partial\xi}\right)^2\right) + \frac{\beta^2}{12}\left(-\gamma^2\bar{C}_{12}\frac{\partial^4\bar{w}}{\partial\theta^4} - \bar{C}_{66}\beta^2\frac{\partial^4\bar{w}}{\partial\xi^2\partial\theta^2}\right) - \beta\bar{C}_{22}\left(\beta\frac{\partial\bar{v}}{\partial\theta} + \beta\bar{w} + \frac{\beta^2}{2}\left(\frac{\partial\bar{w}}{\partial\theta}\right)^2\right)$$

$$+\left(K_w\right)\overline{w}+C_d\dot{\overline{w}}-\left(K_g\right)\left(\gamma\frac{\partial^2\overline{w}}{\partial\xi^2}+\beta\frac{\partial^2\overline{w}}{\partial\theta^2}\right)$$
$$-\left[\frac{\partial^2\overline{w}}{\partial\bar{t}^2}+2\gamma V_x\frac{\partial^2\overline{w}}{\partial\xi\partial\bar{t}}+\gamma^2 V_x{}^2\frac{\partial^2\overline{w}}{\partial\xi^2}\right] \tag{36}$$
$$-\overline{\mu}\left[\gamma^2\frac{\partial^3\overline{w}}{\partial\xi^2\partial\bar{t}}+V_x\gamma^3\frac{\partial^3\overline{w}}{\partial\xi^3}+\beta^2\left(\frac{\partial^3\overline{w}}{\partial\theta^2\partial\bar{t}}+V_x\gamma\frac{\partial^3\overline{w}}{\partial\theta^2\partial\xi}\right)\right]=\frac{\partial^2\overline{w}}{\partial\bar{t}^2}.$$

The border conditions are as the following in the two ends of the tube:

√ **Clamped- Clamped**

$$\begin{aligned} &w=v=u=0 \qquad @ \quad x=0,L \\ &\frac{\partial w}{\partial x}=0 \qquad @ \quad x=0,L \end{aligned} \tag{37}$$

√ **Clamped-Simple**

$$\begin{aligned} &w=v=u=\frac{\partial w}{\partial x}=0 \qquad @ \quad x=0 \\ &w=v=\frac{\partial^2 w}{\partial x^2}=0 \qquad @ \quad x=L \end{aligned} \tag{38}$$

√ **Simple-Simple**

$$\begin{aligned} &w=v=\frac{\partial^2 w}{\partial x^2}=0 \qquad @ \quad x=0 \\ &w=v=\frac{\partial^2 w}{\partial x^2}=0 \qquad @ \quad x=L \end{aligned} \tag{39}$$

The coefficients of tube elasticity, fluid density and fluid viscosity should be made equivalent in the gained equations because there are two phases of background and reinforcement in the tube and there are two phases of water and nanoparticles mixed in the water for the fluid. Mori-Tanaka model is used to make the elastic properties of the tube equivalent by considering the accumulation features of the nanotube. Mixing law is used to make the tube density, fluid density and fluid viscosity equivalent as well.

3. Mori-Tanaka model

In this section, the elastic properties and coefficients of the polymeric composite reinforced by the single walled carbon nanotubes are analyzed micromechanically. Some case like direct regular carbon nanotubes as well as two models of accumulation are analyzed by considering the effect of volumetric fraction and the micromechanical model. It is assumed that polymer is elastic and isotropic and its Young module and Poisson ratio are E_m and v_m respectively. It is assumed that the yarns of the single walled carbon nanotubes are long, orderly, in a same row and with the transverse elastic properties. So, the considered polymeric composite has got transverse elastic properties. Therefore, the strain- tension relationship is as follows in the local coordinates of an initial element (Shi and Feng 2004)

$$\begin{Bmatrix}\sigma_{11}\\ \sigma_{22}\\ \sigma_{33}\\ \sigma_{23}\\ \sigma_{13}\\ \sigma_{12}\end{Bmatrix}=\begin{bmatrix}k+m & l & k-m & 0 & 0 & 0\\ l & n & l & 0 & 0 & 0\\ k-m & l & k+m & 0 & 0 & 0\\ 0 & 0 & 0 & p & 0 & 0\\ 0 & 0 & 0 & 0 & m & 0\\ 0 & 0 & 0 & 0 & 0 & p\end{bmatrix}\begin{Bmatrix}\varepsilon_{11}\\ \varepsilon_{22}\\ \varepsilon_{33}\\ \gamma_{23}\\ \gamma_{13}\\ \gamma_{12}\end{Bmatrix} \tag{40}$$

where k,l,m,n,p are Hill elastic module; k: planestrain volumetric module which is vertical to the yarns, n: non-axial tensile module in the length direction of the yarns, l : cross dependent module, m and p are the shear modules in the planes parallel and verticle to the direction of the yarns, respectively. Hill elastic modules are as the below relationships by Mori- Tanaka method

$$\begin{aligned}
k&=\frac{E_m\{E_m c_m+2k_r(1+v_m)[1+c_r(1-2v_m)]\}}{2(1+v_m)[E_m(1+c_r-2v_m)+2c_m k_r(1-v_m-2v_m^2)]}\\
l&=\frac{E_m\{c_m v_m[E_m+2k_r(1+v_m)]+2c_r l_r(1-v_m^2)]\}}{(1+v_m)[E_m(1+c_r-2v_m)+2c_m k_r(1-v_m-2v_m^2)]}\\
n&=\frac{E_m^2 c_m(1+c_r-c_m v_m)+2c_m c_r(k_r n_r-l_r^2)(1+v_m)^2(1-2v_m)}{(1+v_m)[E_m(1+c_r-2v_m)+2c_m k_r(1-v_m-2v_m^2)]}\\
&\quad+\frac{E_m[2c_m^2 k_r(1-v_m)+c_r n_r(1+c_r-2v_m)-4c_m l_r v_m]}{E_m(1+c_r-2v_m)+2c_m k_r(1-v_m-2v_m^2)}\\
p&=\frac{E_m[E_m c_m+2p_r(1+v_m)(1+c_r)]}{2(1+v_m)[E_m(1+c_r)+2c_m p_r(1+v_m)]}\\
m&=\frac{E_m[E_m c_m+2m_r(1+v_m)(3+c_r-4v_m)]}{2(1+v_m)\{E_m[c_m+4c_r(1-v_m)]+2c_m m_r(3-v_m-4v_m^2)\}}
\end{aligned} \tag{41}$$

where k_r, l_r, n_r, p_r, m_r are Hill elasticity module in the reinforced phase (Shi and Feng 2004). The empirical results show that most of the carbon nanotubes lie as a curve in polymers. It is observed that a great part of carbon nanotubes are concentrated in one place in the composite which is assumed to be spherical and so called “inclusion”. It has properties different from that of its surrounding material. V_r is the final volume of carbon nanotubes. We have

$$V_r=V_r^{inclusion}+V_r^m \tag{42}$$

whereV_r^m, $V_r^{inclusion}$ are respectively a volume of the carbon nanotube in the polymer and inclusion. Two following parameters are used to show the effect of accumulation in the micromechanical model

$$\xi=\frac{V_{inclusion}}{V}, \tag{43}$$

$$\zeta=\frac{V_r^{inclusion}}{V_r}. \tag{44}$$

C_r, the mean volumetric fraction of carbon nanotubes is expressed as

$$C_r=\frac{V_r}{V}. \tag{45}$$

in composite. The relationship between the volumetric fractions of nanotubes in inclusion and polymer is as the following using above relationships

$$\frac{V_r^{inclusion}}{V_{inclusion}} = \frac{C_r \zeta}{\xi}, \quad (46)$$

$$\frac{V_r^m}{V - V_{inclusion}} = \frac{C_r(1-\zeta)}{1-\xi}. \quad (47)$$

Assuming that carbon nanotubes are transverse isotropic, and randomly lie in the inclusion, the inclusion is assumed isotropic. The volumetric module $K$and shear module G is as Eqs. (48) and (49) using Mori- Tanaka method

$$K = K_{out}\left[1 + \frac{\xi\left(\frac{K_{in}}{K_{out}} - 1\right)}{1 + \alpha(1-\xi)\left(\frac{K_{in}}{K_{out}} - 1\right)}\right], \quad (48)$$

$$G = G_{out}\left[1 + \frac{\xi\left(\frac{G_{in}}{G_{out}} - 1\right)}{1 + \beta(1-\xi)\left(\frac{G_{in}}{G_{out}} - 1\right)}\right], \quad (49)$$

where K_{in} and K_{out} are the volumetric module of inclusion and that of composite minus inclusion, respectively. In the same manner, G_{in} and G_{out} are the volumetric module of inclusion and that of composite minus inclusion, respectively which are gained by the following relationships

$$K_{in} = K_m + \frac{(\delta_r - 3K_m\chi_r)C_r\zeta}{3(\xi - C_r\zeta + C_r\zeta\chi_r)}, \quad (50)$$

$$K_{out} = K_m + \frac{C_r(\delta_r - 3K_m\chi_r)(1-\zeta)}{3[1-\xi - C_r(1-\zeta) + C_r\chi_r(1-\zeta)]}, \quad (51)$$

$$G_{in} = G_m + \frac{(\eta_r - 3G_m\beta_r)C_r\zeta}{2(\xi - C_r\zeta + C_r\zeta\beta_r)}, \quad (52)$$

$$G_{out} = G_m + \frac{C_r(\eta_r - 3G_m\beta_r)(1-\zeta)}{2[1-\xi - C_r(1-\zeta) + C_r\beta_r(1-\zeta)]}, \quad (53)$$

where χ_r, β_r, δ_r, η_r are

$$\chi_r = \frac{3(K_m + G_m) + k_r - l_r}{3(k_r + G_m)}, \quad (54)$$

$$\beta_r = \frac{1}{5}\left\{\frac{4G_m + 2k_r + l_r}{3(k_r + G_m)} + \frac{4G_m}{(p_r + G_m)} + \frac{2[G_m(3K_m + G_m) + G_m(3K_m + 7G_m)]}{G_m(3K_m + G_m) + m_r(3K_m + 7G_m)}\right\}, \quad (55)$$

$$\delta_r = \frac{1}{3}\left[n_r + 2l_r + \frac{(2k_r - l_r)(3K_m + 2G_m - l_r)}{k_r + G_m}\right], \quad (56)$$

$$\eta_r = \frac{1}{5}\left[\frac{2}{3}(n_r - l_r) + \frac{4G_m p_r}{(p_r + G_m)} + \frac{8G_m m_r(3K_m + 4G_m)}{3K_m(m_r + G_m) + G_m(7m_r + G_m)} + \frac{2(k_r - l_r)(2G_m + l_r)}{3(k_r + G_m)}\right]. \quad (57)$$

K_m, G_m are the volumetric and shear module of the base phase

$$K_m = \frac{E_m}{3(1-2\upsilon_m)}, \quad (58)$$

$$G_m = \frac{E_m}{2(1+\upsilon_m)}. \quad (59)$$

In addition, β, α in Eqs. (48) and (49) are obtained by

$$\alpha = \frac{(1+\upsilon_{out})}{3(1-\upsilon_{out})}, \quad (60)$$

$$\beta = \frac{2(4-5\upsilon_{out})}{15(1-\upsilon_{out})}, \quad (61)$$

$$\upsilon_{out} = \frac{3K_{out} - 2G_{out}}{6K_{out} + 2G_{out}}. \quad (62)$$

Having the volumetric module K and shear module G of nano composite by the above relationships, E and υ in the isotropic composite material is gained by

$$E = \frac{9KG}{3K + G}, \quad (63)$$

$$\upsilon = \frac{3K - 2G}{6K + 2G}. \quad (64)$$

Having E and υ, the hardness construct matrix is calculated.

4. Mixing law

Mixing law is used to calculate the properties equivalent to the tube density and fluid density and viscosity. Tube equivalent density is as follows according to the mixing law

$$\rho = V_{CNT}\rho_r + (1 - V_{CNT})\rho_m, \quad (65)$$

where ρ_m and ρ_r are the densities of background and nanotube, respectively. V_{CNT} is the volumetric percent of the nanotube in the tube. According to the mixing law, fluid equivalent density and viscosity of the iron oxide nanoparticle with the diameter of 28 nanometers is

$$\rho_f = V_{np}\rho_{np} + (1 - V_{np})\rho_{fluid}, \quad (66)$$

$$\mu = (1 + 7.3V_{np} + 123V_{np}^2)\mu_{fluid}, \quad (67)$$

where ρ_{fluid} and ρ_{np} are respectively the density of the fluid and nanoparticles, μ_{np} and μ_{fluid} are respectively the viscosity of the fluid and nanoparticles and V_{np} is the volumetric percent of the nanoparticles in the fluid.

5. DQM method

DQM is one of the numerical methods in which the governing differential equations are converted to the first order algebraic equations by the weight ratios so that derivative is expressed as a linear sum of weight ratios in a point and the functional amounts there and the other range points in the direction of the coordinate axes. The main relationships of these methods are expressed as the following for a single case (Kolahchi *et al*. 2015, 2016a, 2016b, 2017, Zamanian 2017)

$$\frac{d^n f_x(x_i,\theta_j)}{dx^n}=\sum_{k=1}^{N_x}A_{ik}^{(n)}f(x_k,\theta_j) \qquad n=1,\dots,N_x-1. \tag{68}$$

$$\frac{d^m f_y(x_i,\theta_j)}{d\theta^m}=\sum_{l=1}^{N_\theta}B_{jl}^{(m)}f(x_i,\theta_l) \qquad m=1,\dots,N_\theta-1. \tag{69}$$

$$\frac{d^{n+m} f_{xy}(x_i,\theta_j)}{dx^n d\theta^m}=\sum_{k=1}^{N_x}\sum_{l=1}^{N_\theta}A_{ik}^{(n)}B_{jl}^{(m)}f(x_k,\theta_l). \tag{70}$$

So, it is observed that Selection of the sample points and weight ratios are two very important and determining factors in the accuracy of DQM method which will be mentioned later. Chebyshev polynomial is widely used for solving the engineering problems and produces good results which is expressed as

$$X_i=\frac{L}{2}\left[1-\cos\left(\frac{i-1}{N_x-1}\right)\pi\right] \qquad i=1,\dots,N_x \tag{71}$$

$$\theta_i=\frac{2\pi}{2}\left[1-\cos\left(\frac{i-1}{N_\theta-1}\right)\pi\right] \qquad i=1,\dots,N_\theta \tag{72}$$

The weight ratios are generalized as below for the two dimension case:

a) for the first order derivative

$$A_{ij}^{(1)}=\begin{cases}\dfrac{M(x_i)}{(x_i-x_j)M(x_j)} & for \quad i\neq j, \quad i,j=1,2,\dots,N_x\\ -\sum\limits_{\substack{j=1\\ i\neq j}}^{N_x}A_{ij}^{(1)} & for \quad i=j, \quad i,j=1,2,\dots,N_x\end{cases} \tag{73}$$

$$B_{ij}^{(1)}=\begin{cases}\dfrac{P(\theta_i)}{(\theta_i-\theta_j)P(\theta_j)} & for \quad i\neq j, \quad i,j=1,2,\dots,N_\theta,\\ -\sum\limits_{\substack{j=1\\ i\neq j}}^{N_\theta}B_{ij}^{(1)} & for \quad i=j, \quad i,j=1,2,\dots,N_\theta\end{cases} \tag{74}$$

where

$$M(x_i)=\prod_{\substack{j=1\\ j\neq i}}^{N_x}(x_i-x_j) \tag{75}$$

$$P(\theta_i)=\prod_{\substack{j=1\\ j\neq i}}^{N_\theta}(\theta_i-\theta_j) \tag{76}$$

b) for higher derivative

$$A_{ij}^{(n)}=n\left(A_{ii}^{(n-1)}A_{ij}^{(1)}-\frac{A_{ij}^{(n-1)}}{(x_i-x_j)}\right) \tag{77}$$

$$B_{ij}^{(m)}=m\left(B_{ii}^{(m-1)}B_{ij}^{(1)}-\frac{B_{ij}^{(m-1)}}{(\theta_i-\theta_j)}\right) \tag{78}$$

Using the following time modes, the terms with the time derivative are omitted and the differential equations will be entirely based on the local derivatives.

$$\begin{aligned}\bar{u}(x,y,t)&=\bar{u}(x,y)e^{\lambda\bar{t}},\\ \bar{v}(x,y,t)&=\bar{v}(x,y)e^{\lambda\bar{t}},\\ \bar{w}(x,y,t)&=\bar{w}(x,y)e^{\lambda\bar{t}},\end{aligned} \tag{79}$$

where λ refers to frequency and $\bar{u}(x,y)$, $\bar{v}(x,y)$ and $\bar{w}(x,y)$ show the vibration ranges in three directions of length, circumference and transverse. So, the governing equations and the border condition is written as below in a matrix form

$$\left(\left[\underbrace{K_L+K_{NL}}_{K}\right]+\Omega[C]+\Omega^2[M]\right)\begin{Bmatrix}\{d_b\}\\ \{d_d\}\end{Bmatrix}=0, \tag{80}$$

in which $\Omega=\frac{\lambda}{h}\sqrt{C_{11}/\rho}$ refers the dimensionless frequency. $[K_L]$, $[K_{NL}]$, $[C]$ and $[M]$ show the linear part of the hardness matrix, the nonlinear part of the hardness matrix, Damper matrix and mass matrix, respectively. $\{d_b\}$ & $\{d_d\}$ are the dynamic range vectors in points of the border and field term

$$\{d_b\}=\{\bar{u}_{i1},\bar{v}_{i1},\bar{w}_{i1},\bar{w}_{i2},\bar{u}_{iN_\theta},\bar{v}_{iN_\theta},\bar{w}_{iN_\theta},\bar{w}_{i(N_\theta-1)}\} \qquad i=1,\dots,N_x \tag{81}$$

$$\{d_d\}=\{\bar{u}_{ij},\bar{v}_{ij},\bar{w}_{i(j+1)}\} \qquad i=1,\dots,N_x,\ j=2,\dots,N_x-1 \tag{82}$$

The above equation is in the total form of aeigenvalue problem but should be converted to the standard form of a eigenvalue problem to be solved. So, Eq. (80) is changed to (83) by defining the change of variable $d'=\Omega d_{eq}$

$$[A]\{Z\}=\Omega\{Z\}, \tag{83}$$

where

$$[A]=\begin{bmatrix}[0] & [I]\\ -[M^{-1}K] & -[M^{-1}C]\end{bmatrix} \tag{84}$$

$$\{Z\}=\begin{Bmatrix}\{(d\ )_b\}\\ \{(d\ )_d\}\\ \{(d')_b\}\\ \{(d')_b\}\end{Bmatrix} \tag{85}$$

n which $[I]$ shows the identity matrix and $\{d'\}$ is the derivative of the movement vectors or vibration range. The mentioned equation is aeigenvalue problem which is solved as follows:

- Nonlinear terms are ignored in the hardness matrix and the special vector (the movement vector $\{z\}$) and the eigenvalue (Ω) are calculated in the linear manner.
- The movement vectors in the previous step are placed in the nonlinear terms of the hardness matrix and the eigenvalue and special vector of the nonlinear term are calculated again.
- This process is continued until below convergence ratio is satisfied.

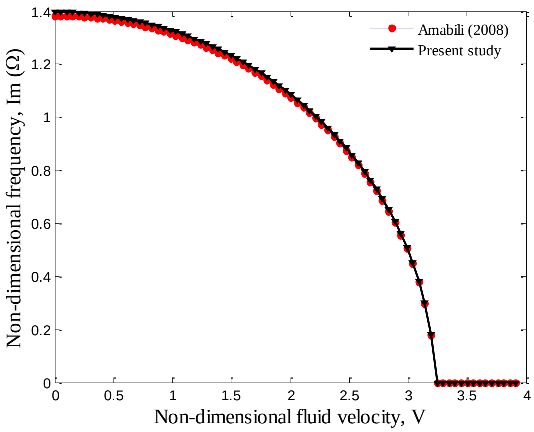

Fig. 2 Validation of imaginary part of frequency

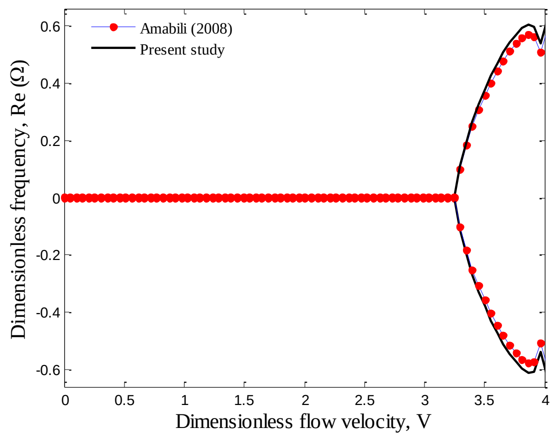

Fig. 3 Validation of real part of frequency

$$\frac{\alpha_{i-1} - \alpha_i}{\alpha_{i-1}} < 0.01\% \tag{86}$$

It should be mentioned that α means system frequency.

6. Results

The numerical results of the vibrations and instability in the tube reinforced by the carbon nanotubes having fluid mixed with the nanoparticles were analyzed in this section. In this study, the tube is simulated by the cylindrical shell model located in the viscoelastic area. The numerical method of Square differences is used due to the nonlinear nature of the equations. This study is aimed to analyze the effect of nanoparticles of the fluid, geometric parameters of tube, viscoelastic area, volumetric percent of carbon nanotube and the accumulation of nanotubes on the frequency and critical velocity of the fluid. The material of the pipe is made of elastic module E_m=125 GPa, Poisson ratio v_m=0.3 and density ρ_m=1.45 Kg/m^3. Elastic module and Poisson ratio of carbon nanotubes are E_r=1 TPa and v_r=0.3, respectively with length to radius ratio of L/R=2 and thickness to radius ratio of h/R=0.02. The density of the fluid in the water tube is ρ_{fluid}=998.2 Kg/m^3 and its viscosity is $\mu_{fluid}=1\times10^{-3}$ Pa.s. It has iron oxide nanoparticles with the density of ρ_{np}=3970 Kg/m^3 .

6.1 Validation

In this section, it is used algorithm to test the accuracy. The graph for the effect of dimensionless velocity of the fluid ($u_f=V/\{\pi^2/L[D/\rho h]\}^{0.5}$) on the imaginary and real part of the dimensionless frequency ($\omega=\lambda/\{\pi^2/L^2[D/\rho h]\}^{0.5}$) is shown in Figs. 2 and 3, respectively and is compared with the research of Amabili (2008). The parameters considered for accuracy testing are the same as those in Amabili's research (2008) which is shell without carbon nanotube and nanoparticles and with the elasticity module of E=206 GPa, Poisson ratio v=0.3, density ρ=7850 Kg/m^3, length to radius L/R=2, thickness to radius h/R=0.01 and with the fluid of water. Results show a relative good agreement between the

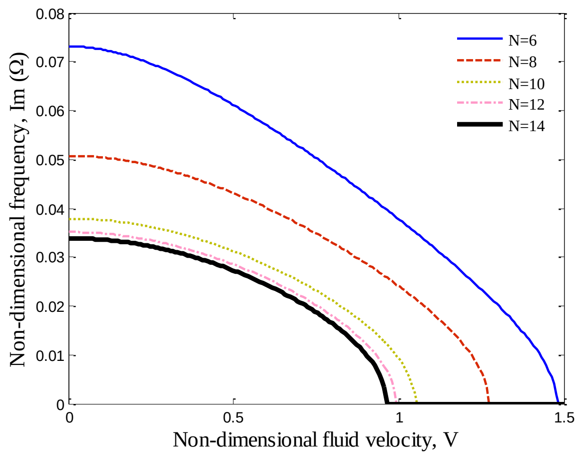

Fig. 4 Convergence of DQM for imaginary part of frequency

present research and Amabili (2008).

6.2 Convergence of numerical method

Figs. 4 and 5 show the convergence and accuracy of square differences method to obtain the imaginary and real part of the dimensionless eigenvalue against the dimensionless velocity of the fluid. Chebychev polynomial is used to choose the points in the network about which is explained in part 3. It is clearly seen that there is a fast convergence ratio for the solution method on the imaginary and real part of the dimensionless eigenvalue and the answers reach to a desirable convergence for 14 points. Therefore, the number of the points is considered 14 to extract the results in this research.

6.3 The effect of the different parameters

In this section, it is going to analyze the effects of nanoparticles of the fluid, tube's geometric parameters, viscoelastic area, the volumetric percent of carbon nanotube and accumulation of nanotube on the frequency and critical velocity of the fluid. In the given graphs, the imaginary part of the eigenvalue shows the frequency and its real part shows damping of the construct.

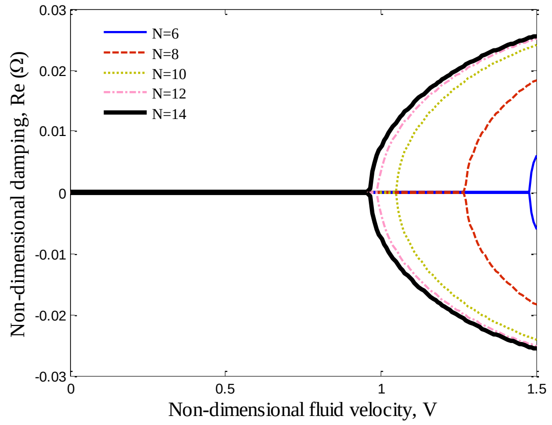

Fig. 5 Convergence of DQM for real part of frequency

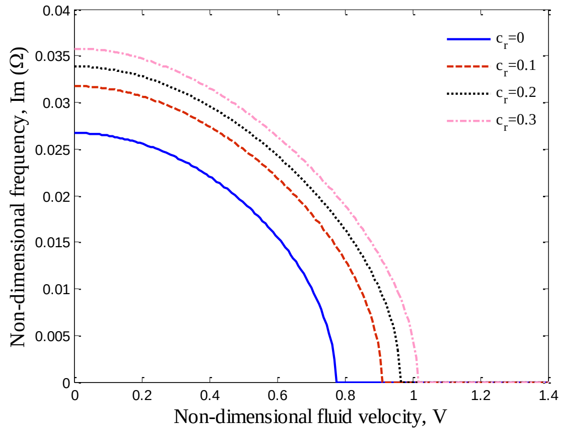

Fig. 6 The effect of volume percent of SWCNTs on the imaginary part of frequency

Figs. 6 and 7 show the effect of the volume percent of the carbon nanotubes on the frequency (Im(Ω)) and system damping (Re(Ω)) according to the fluid velocity (V) in a dimensionless manner. As it can be seen, as the velocity of the fluid increases, the imaginary part of the eigenvalue decreases. There is an equal amount with an opposite sign for the real parts of the eigenvalue from this velocity on. Its positive root causes divergence instability in the system. The velocity in which the imaginary and real part of the eigenvalue get zero is called the critical velocity of the fluid. It is observed that the volumetric percent of carbon nanotubes greatly effects on the vibrations and instability of the system. As the volumetric percent of carbon nanotubes increases, frequency (the imaginary part of the eigenvalue) and critical velocity of the fluid increase due to the increase of construct's hardness by the increase in the volumetric percent of carbon nanotubes.

The effect of agglomeration in carbon nanotubes in a special part on the imaginary and real part of the eigenvalue is shown respectively in Figs. 8 and 9 according to the fluid velocity in a dimensionless velocity. As it can be seen, accumulation decreases the hardness of the construct so the frequency and critical velocity of the fluid will decrease. The results in this graph can be very important due to this fact that the uniform distribution of the nanotubes is impossible in making the nano composite constructs.

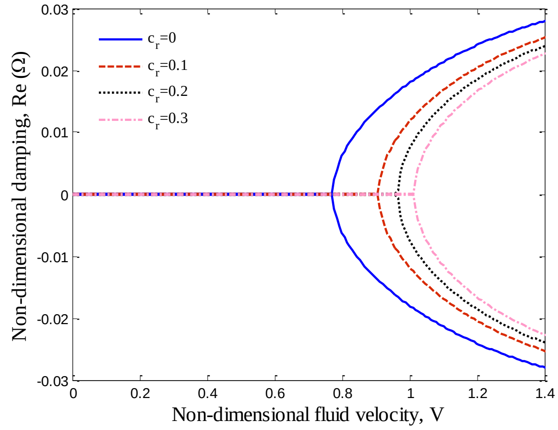

Fig. 7 The effect of volume percent of SWCNTs on the real part of frequency

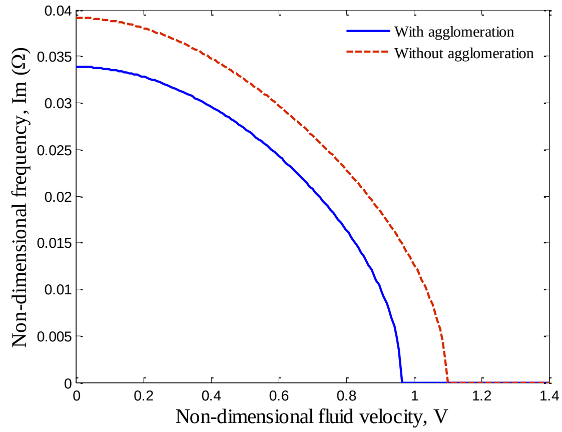

Fig. 8 The effect of agglomeration of SWCNTs on the imaginary part of frequency

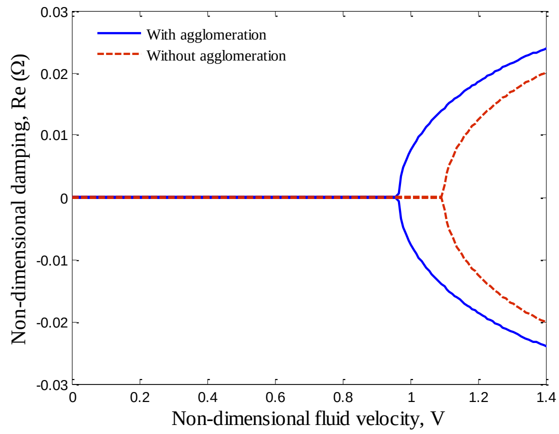

Fig. 9 The effect of agglomeration of SWCNTs on the real part of frequency

Consequently, the less the accumulation in the different points, the more the frequency and critical velocity of the fluid to reinforce the tube by the nanotubes.

Figs. 10 and 11 show the effect of volume percent of the nanoparticles in the accumulation volume on the frequency and damping of the construct based on the fluid velocity, respectively. As it can be seen, there is a direct relationship

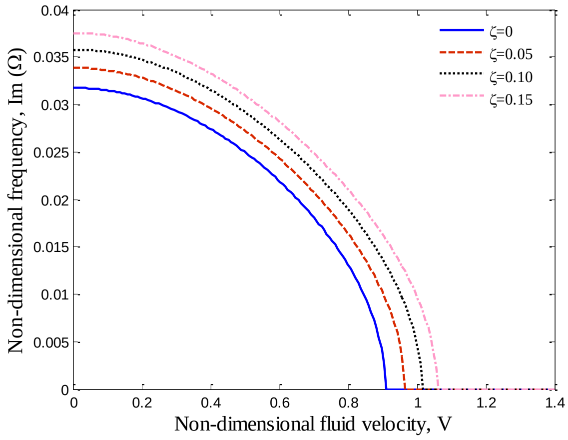

Fig. 10 The effect of volume percent of the nanoparticles in the accumulation volume on the imaginary part of frequency

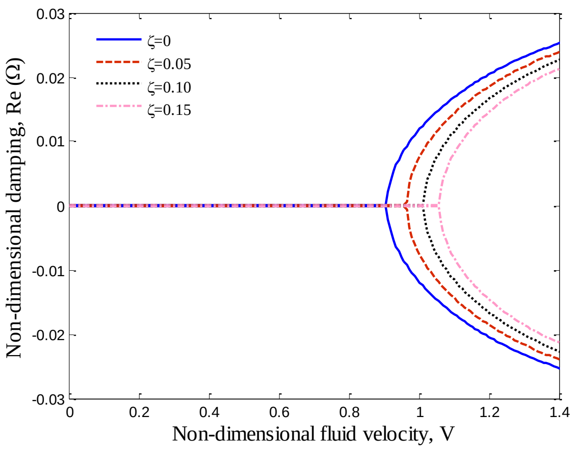

Fig. 11 The effect of volume percent of the nanoparticles in the accumulation volume on the real part of frequency

between the changes in the volumetric percent of the nanoparticles and accumulation, frequency changes and critical velocity of the fluid so that as the volumetric percent of the nanotubes increases in the accumulation, the frequency and critical velocity of the fluid will increase too. In another word, the decrease of the volumetric percent of the nanoparticles in the accumulation volume delays the instability of the tube caused by the passage of the fluid.

The effect of thickness to length ratio ($\gamma=h/L$) of the tube on the imaginary and real part of the dimensionless eigenvalue is shown respectively in Figs. 12 and 13 based on the velocity of the dimensionless fluid. It can be understood that the increase in the thickness-length ratio increases the frequency and critical velocity of the fluid which is due to the increasing hardness of the system.

Figs. 14 and 15 show the effect of thickness to radius ratio of the tube ($\beta=h/R$) on the frequency and damping of the construct against the dimensionless velocity of the fluid. The results show that as this ratio increases, so does the hardness of the tube so the frequency and critical velocity of the fluid increase.

The effect of volume percent of iron oxide nanoparticles in the fluid on the vibrations of the construct is discussed in

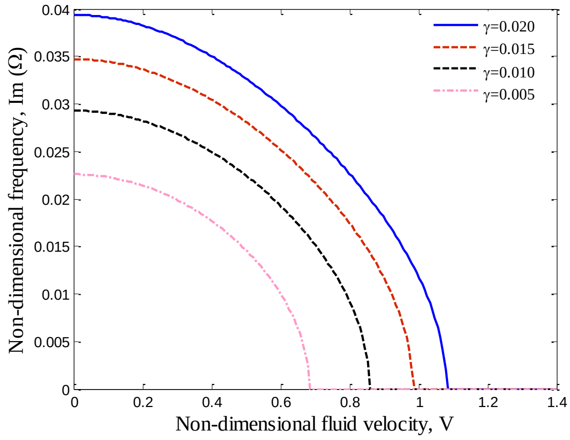

Fig. 12 The effect of thickness to length ratio on the imaginary part of frequency

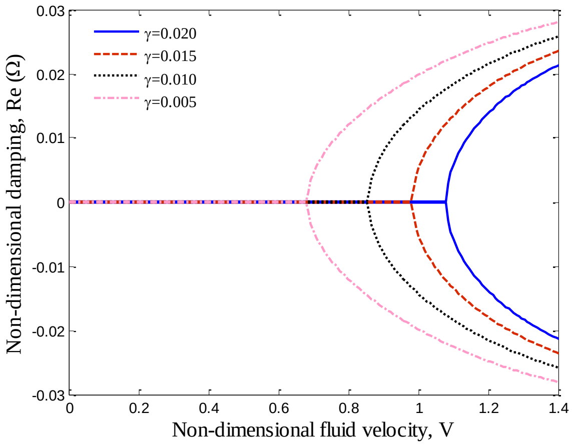

Fig. 13 The effect of thickness to length ratio on the real part of frequency

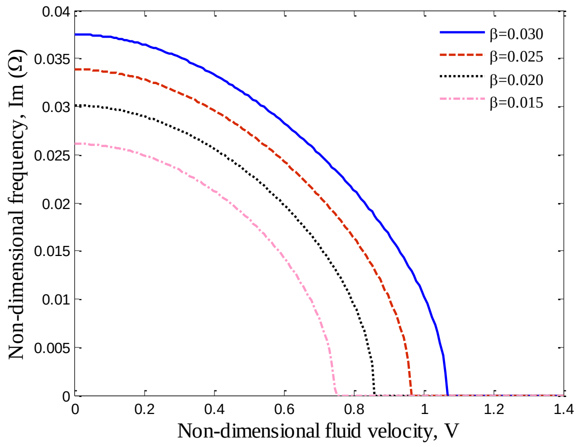

Fig. 14 The effect of thickness to radius ratio on the imaginary part of frequency

this section. Figs. 16 and 17 shows the imaginary part of the dimensionless eigenvalue and the real part of the dimensionless eigenvalue against the dimensionless velocity of the fluid, respectively. It is observed that as the volumetric percent of the iron oxide nanoparticles increases in the fluid, the frequency and the critical velocity of the

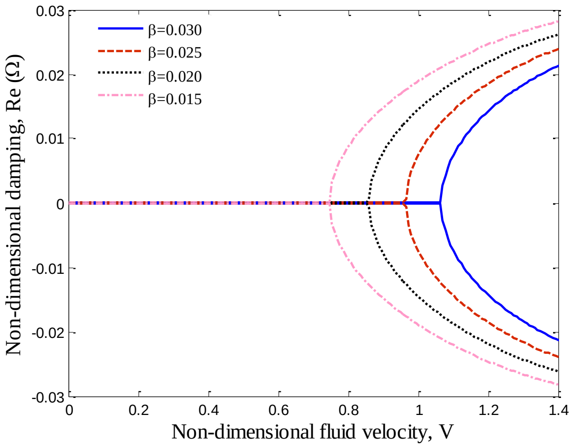

Fig. 15 The effect of thickness to radius ratio on the real part of frequency

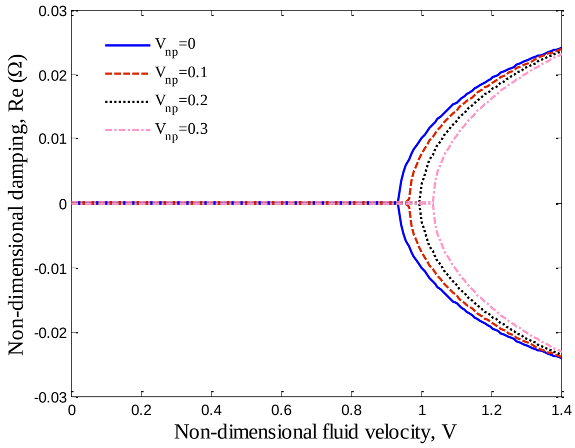

Fig. 17 The effect of volume percent of iron oxide nanoparticles in the fluid on the real part of frequency

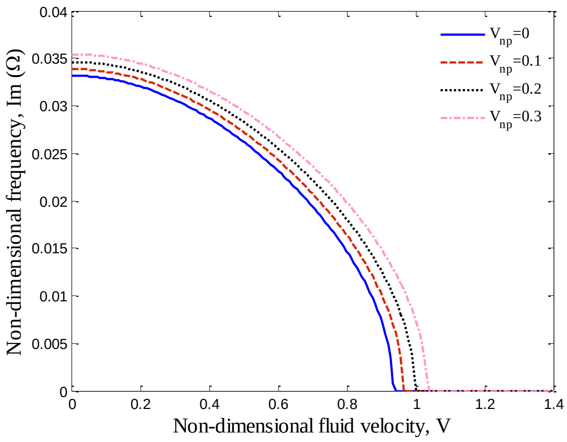

Fig. 16 The effect of volume percent of iron oxide nanoparticles in the fluid on the imaginary part of frequency

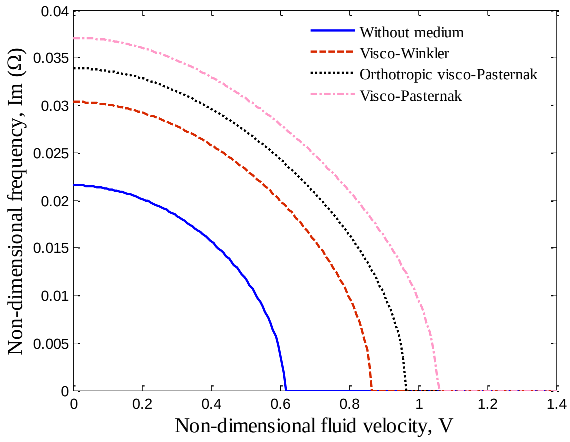

Fig. 18 The effect of viscoelastic medium on the imaginary part of frequency

fluid will increase because as the volumetric percent of iron oxide particles increases in the fluid, the velocity of the fluid decreases and the damping caused in the construct decreases. So, as the damping decreases, its frequency and critical velocity increase.

The effect of the viscoelastic area is considered as the vertical spring (Winkler), shear layer (Pasternak) and damping ratio. Four aspects are considered to show this effect:

• without viscoelastic area

• Visco-Winkler area without considering Pasternak shear module

• orthotropic Visco- Pasternak area

• Visco- Pasternak area

The effect of viscoelastic medium on the frequency and damping of the construct is shown respectively in Figs. 18 and 19 against the dimensionless velocity of the fluid. It is observed that the bed in which the system is located considerable effects on its vibrations and instability of the system so that if the area is considered viscoelastic, the frequency and the critical velocity of the fluid will increase. As it can be seen, the critical velocity of the fluid follows the following arrangement in the various areas:

Visco-Pasternak< orthotropic Visco- Pasternak<Visco-Winkler< without area

The effect of Pasternak area is more than that of Winkler generally since it considers the effect of the shear layer besides the vertical springs. In addition, the critical velocity and frequency of the fluid decrease while using the orthotropic area because the shear layer is considered in the 45°angle.

The imaginary and real parts of the frequency for the eigenvalue are shown in the Figs. 20 and 21 according to the velocity of the fluid for different boundary conditions, respectively. It is observed that the kind of the support severely effects on the instability of the system. As it can be seen, there is a less movement freedom for the system with the clamped support due to its two bounded ends and frequency and critical velocity of fluid is more in it than those in the other supports. Generally, the critical velocity of the fluid is based on the following order in the different border conditions:

clamped-clamped > clamped-Simple> Simple-Simple

7. Conclusions

This research analyzed the vibrations and instability in a

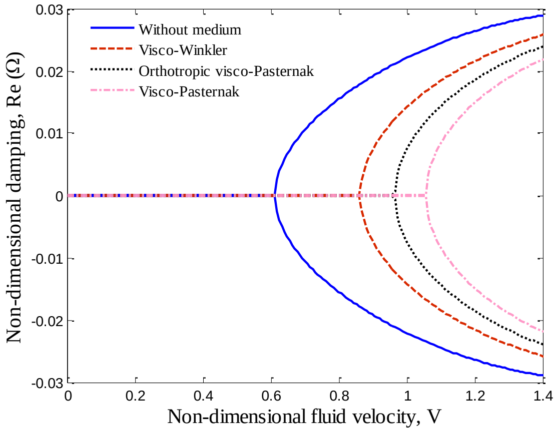

Fig. 19 The effect of viscoelastic medium on the real part of frequency

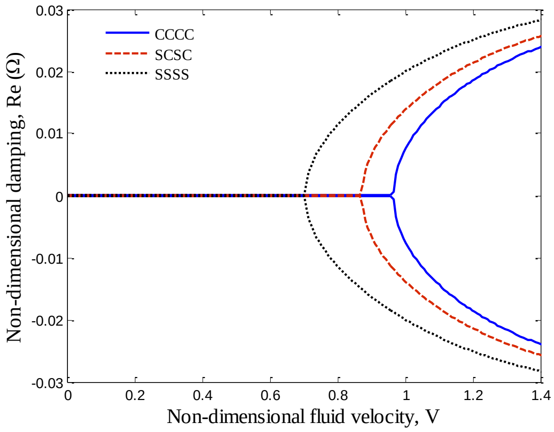

Fig. 21 The effect of different boundary conditions on the real part of frequency

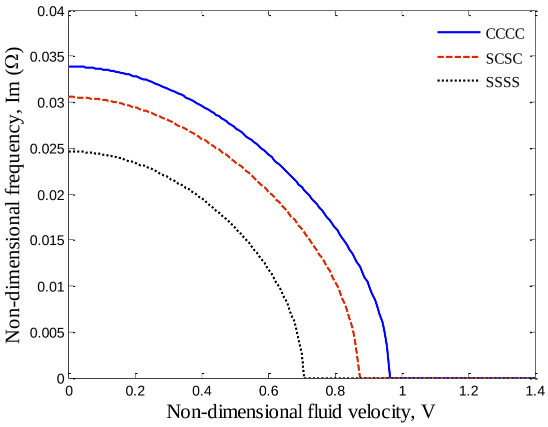

Fig. 20 The effect of different boundary conditions on the imaginary part of frequency

polymer tube reinforced by the carbon nanotube located in a viscoelastic area with fluid current mixed with the nanoparticles. Mori- Tanaka model is used to model and determine composite equivalent mechanical properties and to consider the accumulation property. Navier-Stocks equation is applied to extract the force caused by the fluid in the tube and mixing law was used to consider the effect of nanoparticles of the fluid. The movement equations were extracted using nonlinear strain- shift equation, tension-strain equation, energy method and Hamilton principle. This research is aimed to analyze the effect of volumetric percent of carbon nanotube, tube accumulation, viscoelastic area, volumetric percent of the nanoparticles in the fluid, fluid velocity and the geometric parameters of the tube on the frequency and critical velocity of the fluid. The final results of this research are:

• Considering 14 network points leads to the convergence of the results
• The imaginary and real parts of the eigenvalue reach zero simultaneously in a special amount of the fluid velocity called the critical velocity.
• As the volumetric percent of carbon nanotubes increases, the frequency (the imaginary part of eigenvalue) and critical velocity of the fluid will increase too.
• Considering accumulation decreases the hardness of the construct and so do the frequency and critical velocity of the fluid.
• The more the volumetric percent of the nanotubes in accumulation, the more the frequency and critical velocity of the fluid.
• The increase of thickness- length ratio causes the increase of the frequency and critical velocity of the fluid.
• As the thickness- radius ratio of the tube increases, the tube hardness increases too and the frequency and critical velocity of the fluid increase.
• As the volumetric percent of the iron oxide nanoparticles increases in the fluid, the frequency and critical velocity of the fluid will increase.
• The effect of Pastrnak area is more than that of Winkler since it considers the effect of the shear layer besides that of the vertical spring.
• The frequency and critical velocity of the fluid get less while using the orthotropic area because the shear layer is considered 45°.
• There are less movement freedom and higher frequency and critical velocity in the fluid in the system with the tight supports than the other supports due to being bounded in two ends.

References

Ahouel, M., Houari, M.S.A., Adda Bedia, E.A. and Tounsi, A. (2016), "Size-dependent mechanical behavior of functionally graded trigonometric shear deformable nanobeams including neutral surface position concept", *Steel Compos. Struct.*, **20**(5), 963-981.

Amabili, M. (2003), "A comparison of shell theories for large-amplitude vibrations of circular cylindrical shells: Lagrangian approach", *J. Sound Vib.*, **264**, 1091-1125.

Amabili, M. (2008), *Nonlinear Vibrations and Stability of Shells and Plates*, Cambridge University Press, New York.

Amabili, M. and Garziera, R. (2002), "Vibrations of circular cylindrical shells with nonuniform constraints, elastic bed and added mass. Part II: shells containing or immersed in axial flow", *J. Fluid. Struct.*, **16**, 31-51.

Attia, A., Tounsi, A., Adda Bedia, E.A. and Mahmoud, S.R. (2015), "Free vibration analysis of functionally graded plates with temperature-dependent properties using various four variable refined plate theories", *Steel Compos. Struct.*, **18**(1), 187-212.

Bahadori, R. and Najafizadeh, M.M. (2015), "Free vibration analysis of two-dimensional functionally graded axisymmetric cylindrical shell on Winkler-Pasternak elastic foundation by First-order Shear Deformation Theory and using Navier-differential quadrature solution methods", *Appl. Math. Model.*, **39**, 4877-4894.

Belabed, Z., Houari, M.S.A., Tounsi, A., Mahmoud, S.R. and Bég, O.A. (2014), "An efficient and simple higher order shear and normal deformation theory for functionally graded material (FGM) plates", *Compos. Part B*, **60**, 274-283.

Beldjelili, Y., Tounsi, A. and Mahmoud, S.R. (2016), "Hygro-thermo-mechanical bending of S-FGM plates resting on variable elastic foundations using a four-variable trigonometric plate theory", *Smart Struct. Syst.*, **18**(4), 755-786.

Belkorissat, I., Houari, M.S.A., Tounsi, A. and Hassan, S. (2015), "On vibration properties of functionally graded nano-plate using a new nonlocal refined four variable model", *Steel Compos. Struct.*, **18**(4), 1063-1081.

Bellifa, H., Benrahou, K.H., Bousahla, A.A., Tounsi, A. and Mahmoud, S.R. (2017), "A nonlocal zeroth-order shear deformation theory for nonlinear postbuckling of nanobeams", *Struct. Eng. Mech.*, **62**(6), 695-702.

Bellifa, H., Benrahou, K.H., Hadji, L., Houari, M.S.A. and Tounsi, A. (2016), "Bending and free vibration analysis of functionally graded plates using a simple shear deformation theory and the concept the neutral surface position", *J Braz. Soc. Mech. Sci. Eng.*, **38**(1), 265-275.

Bennoun, M., Houari, M.S.A. and Tounsi, A. (2016), "A novel five variable refined plate theory for vibration analysis of functionally graded sandwich plates", *Mech. Adv. Mater. Struct.*, **23**(4), 423-431.

Bessaim, A., Houari, M.S.A. and Tounsi, A. (2013), "A new higher-order shear and normal deformation theory for the static and free vibration analysis of sandwich plates with functionally graded isotropic face sheets", *J. Sandw. Struct. Mater.*, **15**(6), 671-703.

Besseghier, A., Houari, M.S.A., Tounsi, A. and Hassan, S. (2017), "Free vibration analysis of embedded nanosize FG plates using a new nonlocal trigonometric shear deformation theory", *Smart Struct. Syst.*, **19**(6), 601-614.

Bochkarev, S.A. and Matveenko, V.P. (2013), "Numerical analysis of stability of a stationary or rotating circular cylindrical shell containing axially flowing and rotating fluid", *Int. J. Mech. Sci.*, **68**, 258-269.

Bouafia, Kh., Kaci, A., Houari M.S.A. and Tounsi, A. (2017), "A nonlocal quasi-3D theory for bending and free flexural vibration behaviors of functionally graded nanobeams", *Smart Struct. Syst.*, **19**, 115-126.

Bouderba, B., Houari, M.S.A. and Tounsi, A. (2013), "Thermomechanical bending response of FGM thick plates resting on Winkler-Pasternak elastic foundations", *Steel Compos. Struct.*, **14**(1), 85-104.

Bouderba, B., Houari, M.S.A., Tounsi, A. and Mahmoud, S.R. (2016b), "Thermal stability of functionally graded sandwich plates using a simple shear deformation theory", *Struct. Eng. Mech.*, **58**(3), 397-422.

Boukhari, A., Atmane, H.A., Tounsi, A., Adda Bedia, E.A. and Mahmoud, S.R. (2016), "An efficient shear deformation theory for wave propagation of functionally graded material plates", *Struct. Eng. Mech.*, **57**(5), 837-859.

Bounouara, F., Benrahou, K.H., Belkorissat, I. and Tounsi, A. (2016), "A nonlocal zeroth-order shear deformation theory for free vibration of functionally graded nanoscale plates resting on elastic foundation", *Steel Compos. Struct.*, **20**(2), 227-249.

Bourada, M., Kaci, A., Houari, M.S.A. and Tounsi, A. (2015), "A new simple shear and normal deformations theory for functionally graded beams", *Steel Compos. Struct.*, **18**(2), 409-423.

Bousahla, A.A., Benyoucef, S., Tounsi, A. and Mahmoud, S.R. (2016a), "On thermal stability of plates with functionally graded coefficient of thermal expansion", *Struct. Eng. Mech.*, **60**(2), 313-335.

Chikh, A., Tounsi, A., Hebali, H. and Mahmoud, S.R. (2017), "Thermal buckling analysis of cross-ply laminated plates using a simplified HSDT", *Smart Struct. Syst.*, **19**(3), 289-297.

Dai, H.L., Wang, L., Qian, Q. and Ni, Q. (2014), "Vortex-induced vibrations of pipes conveying pulsating fluid", *Ocean Eng.*, **77**, 12-22.

De Bellis, M.L., Ruta, G.C. and Elishakoff, I. (2010), "Influence of a Wieghardt foundation on the dynamic stability of a fluid conveying pipe", *Arch. Appl. Mech.*, **80**, 785-801.

Donnell, L.H. (1934), "A new theory for the buckling of thin cylinders under axial compression and bending", *Tran. ASME*, **56**, 795-806.

Draiche, K., Tounsi, A. and Mahmoud, S.R. (2016), "A refined theory with stretching effect for the flexure analysis of laminated composite plates", *Geomech. Eng.*, **11**, 671-690.

Duc, N.D. and Than, P.T. (2015), "Nonlinear dynamic response and vibration of shear deformable imperfect eccentrically stiffened S-FGM circular cylindrical shells surrounded on elastic foundations", *Aero. Sci. Tech.*, **40**, 115-127.

El-Haina, F., Bakora, A., Bousahla, A.A. and Hassan, S. (2017), "A simple analytical approach for thermal buckling of thick functionally graded sandwich plates", *Struct. Eng. Mech.*, **63**(5), 585-595.

Ghorbanpour Arani, A., Karimi, M.S. and Rabani Bidgoli, M. (2016), "Nonlinear vibration and instability of rotating piezoelectric nano-composite sandwich cylindrical shells containing axially flowing and rotating fluid-particle mixture", *Polym. Compos.*, **38**(S1), E577-E596.

Hamidi, A., Houari, M.S.A., Mahmoud, S.R. and Tounsi, A. (2015), "A sinusoidal plate theory with 5-unknowns and stretching effect for thermomechanical bending of functionally graded sandwich plates", *Steel Compos. Struct.*, **18**(1), 235-253.

Kadoli, R. and Ganesan, N. (2003), "Free vibration and buckling analysis of composite cylindrical shells conveying hot fluid", *Compos. Struct.*, **60**, 19-32.

Kamarian, S., Sadighi, M., Shakeri, M. and Yas, M.H. (2014), "Free vibration response of sandwich cylindrical shells with functionally graded material face sheets resting on Pasternak foundation", *J. Sand. Struct. Mater.*, **16**, 511-533.

Khetir, H., Bouiadjra, M.B., Houari, M.S.A., Tounsi, A. and Mahmoud, S.R. (2017), "A new nonlocal trigonometric shear deformation theory for thermal buckling analysis of embedded nanosize FG plates", *Struct. Eng. Mech.*, **64**(4), 391-402.

Kolahchi, R., Hosseini, H. and Esmailpour, M. (2016b), "Differential cubature and quadrature-Bolotin methods for dynamic stability of embedded piezoelectric nanoplates based on visco-nonlocal-piezoelasticity theories", *Compos. Struct.*, **157**, 174-186.

Kolahchi, R., Rabani Bidgoli, M., Beygipoor, Gh. and Fakhar, M.H. (2015), "A nonlocal nonlinear analysis for buckling in embedded FG-SWCNT-reinforced microplates subjected to magnetic field", *J. Mech. Sci. Tech.*, **29**, 3669-3677.

Kolahchi, R., Safari, M. and Esmailpour, M. (2016a), "Dynamic stability analysis of temperature-dependent functionally graded CNT-reinforced visco-plates resting on orthotropic elastomeric medium", *Compos. Struct.*, **150**, 255-265.

Kolahchi, R., Zarei, M.Sh., Hajmohammad, M.H. and Naddaf

Oskouei, A. (2017), "Visco-nonlocal-refined Zigzag theories for dynamic buckling of laminated nanoplates using differential cubature-Bolotin methods", *Thin Wall. Struct*., **113**, 162-169.

Kumarm A., Chakrabartim, A. and Bhargavam, P. (2013), "Vibration of laminated composites and sandwich shells based on higher order zigzag theory", *Eng. Struct*., **56**, 880-888.

Larbi Chaht, F., Kaci, A., Houari M.S.A. and Hassan, S. (2015), "Bending and buckling analyses of functionally graded material (FGM) size-dependent nanoscale beams including the thickness stretching effect", *Steel Compos. Struct.*, **18**(2), 425-442.

Lei, Z.X., Zhang, L.W., Liew, K.M. and Yu, J.L. (2014), "Dynamic stability analysis of carbon nanotube-reinforced functionally graded cylindrical panels using the element-free kp-Ritz method", *Compos. Struct.*, **113**, 328-338.

Leissa, A.W. (1973), *Vibrations of Shells*, NASA SP-288, Washington DC.

Li, Ch., Zhang, Y., Tu, W., Jun, C., Liang, H. and Yu, H. (2017), "Soft measurement of wood defects based on LDA feature fusion and compressed sensor images", *J. Forest. Res*., **28**, 1285-1292.

Li, Y.Q. and Tamura, Y. (2005), "Nonlinear dynamic analysis for large-span single-layer reticulated shells subjected to wind loading", *Wind Struct*., **8**, 35-48.

Liew, K.M., Lei, Z.X., Yu, J.L. and Zhang, L.W. (2014), "Postbuckling of carbon nanotube-reinforced functionally graded cylindrical panels under axial compression using a meshless approach", *Comput. Meth. Appl. Mech. Eng*., **268**, 1-17.

Liu, H., Ma, J. and Huang, W. (2018), "Sensor-based complete coverage path planning in dynamic environment for cleaning robot", *CAAI Trans. Intell. Technol*., **3**, 65-72.

Love, A.E.H. (1892), *A Treatise on the Mathematical Theory of Elasticity*, Cambridge University Press, Dover, New York.

Mahi, A., Bedia, E.A.A. and Tounsi, A. (2015), "A new hyperbolic shear deformation theory for bending and free vibration analysis of isotropic, functionally graded, sandwich and laminated composite plates", *Appl. Math. Model*., **39**, 2489-2508.

Mantari, J.L. and Guedes Soares, C. (2014), "Optimized sinusoidal higher order shear deformation theory for the analysis of functionally graded plates and shells", *Compos. Part B*, **56**, 126-136.

Menasria, A., Bouhadra, A., Tounsi, A. and Hassan, S. (2017), "A new and simple HSDT for thermal stability analysis of FG sandwich plates", *Steel Compos. Struct.*, **25**(2), 157-175.

Messina, A. and Soldatos, K.P. (1999), "Vibration of completely free composite plates and cylindrical shell panels by a higher-order theory", *Int. J. Mech. Sci.*, **41**, 891-918.

Meziane, M.A.A., Abdelaziz, H.H. and Tounsi, A.T. (2014), "An efficient and simple refined theory for buckling and free vibration of exponentially graded sandwich plates under various boundary conditions", *J. Sandw. Struct. Mater.*, **16**(3), 293-318.

Mouffoki, A., Adda Bedia, E.A., Houari, M.S.A. and Hassan, S. (2017), "Vibration analysis of nonlocal advanced nanobeams in hygro-thermal environment using a new two-unknown trigonometric shear deformation beam theory", *Smart Struct. Syst.*, **20**(3), 369-383.

Padhy, S. and Panda, S. (2017), "A hybrid stochastic fractal search and pattern search technique based cascade PI-PD controller for automatic generation control of multi-source power systems in presence of plug in electric vehicles", *CAAI Trans. Intell. Technol*., **2**, 12-25.

Paidoussis, M.P. (2003), *Fluid-Structure Interactions: Slender Structures and Axial Flow*, Elsevier Academic Press, London, UK.

Paidoussis, M.P. and Denise, J.P. (1972), "Flutter of thin cylindrical shells conveying fluid", *J. Sound Vib*., **20**, 9-26.

Paidoussis, M.P., Misra, A.K. and Chan, S.P. (1985), "Dynamics and stability of coaxial cylindrical shells conveying viscous fluid", *J. Appl. Mech*., **52**, 389-396.

Pellicano, F., Amabili, M. and Padoussis, M.P. (2002), "Effect of the geometry on the non-linear vibration of circular cylindrical shells", *Int. J. Nonlin. Mech*., **37**, 1181-1198.

Reddy, J.N. (2004), *Mechanics of Laminated Composite Plates and Shells*, 2nd Edition, CRC Press, Washington.

Rishikeshan, C.A. and Ramesh, H. (2017), "A novel mathematical morphology based algorithm for shoreline extraction from satellite images", *Geo-spatial Inform. Sci.*, **20**, 345-352.

Sanders, J.L. (1959), *An Improved First Approximation Theory for Thin Shells*, NASA TR- R24.

Seo, Y.S., Jeong, W.B., Yoo, W.S. and Jeong, H.K. (2015), "Frequency response analysis of cylindrical shells conveying fluid using finite element method", *J. Mech. Sci. Tech.*, **19**, 625-633.

Shi, D.L. and Feng, X.Q. (2004), "The Effect ofNanotube Waviness and Agglomeration on the Elastic Property of Carbon Nanotube-Reinforced Composite", *J. Eng. Mater. Tech.*, ASME, **126**, 250-270.

Sofiyevm, A.H. (2016), "Nonlinear free vibration of shear deformable orthotropic functionally Tan, P. and Tong, L. (2001), "Micro-electromechanics models for piezoelectric-fiber-reinforced composite materials", *Compos. Sci. Tech.*, **61**, 759-769.

Torres-Jimenez, J. and Rodriguez-Cristerna, A. (2017), "Metaheuristic post-optimization of the NIST repository of covering arrays", *CAAI Trans. Intell. Technol*., **2**, 31-38.

Wang, L. (2009), "A further study on the non-linear dynamics of simply supported pipes conveying pulsating fluid", *Int. J. Nonlin. Mech*., **44**, 115-121.

Weaver, D.S. and Unny, T.E. (1973), "On the dynamic stability of fluid-conveying pipes", *J. Appl. Mech*., **40**, 48-52.

Wen, Q., He, J., Guan, Sh., Chen, T., Hu, Y., Wu, W., Liu, F. and Qiao, Y. (2017), "The TripleSat constellation: a new geospatial data service model", *Geo-spatial Inform. Sci.*, **20**, 163-173.

Wuite, J. and Adali, S. (2005), "Deflection and stress behaviour of nanocomposite reinforced beams using a multiscale analysis", *Compos. Struct*., **71**, 388-396.

Yahia, S.A., Hassen, A.A., Houari, M.S.A. and Tounsi, A. (2015), "Wave propagation in functionally graded plates with porosities using various higher-order shear deformation plate theories", *Struct. Eng. Mech.*, **53**(6), 1143-1165.

Yang, H. and Yu, L. (2017), "Feature extraction of wood-hole defects using wavelet-based ultrasonic testing", *J. Forest. Res*., **28**, 395-402.

Zamanian, M., Kolahchi, R. and Rabani Bidgoli, M. (2017), "Agglomeration effects on the buckling behaviour of embedded concrete columns reinforced with SiO2 nano-particles", *Wind Struct.*, **24**, 43-57.

Zemri, A., Houari, M.S.A., Bousahla, A.A. and Tounsi A. (2015), "A mechanical response of functionally graded nanoscale beam: an assessment of a refined nonlocal shear deformation theory beam theory", *Struct. Eng. Mech*., **54**(4), 693-710.

Zhao, B., Gao, L., Liao, W. and Zhang, B. (2017), "A new kernel method for hyperspectral image feature extraction", *Geo-spatial Inform. Sci.*, **20**, 309-318.

Zidi, M., Tounsi, A. and Bég, O.A. (2014), "Bending analysis of FGM plates under hygro-thermo-mechanical loading using a four variable refined plate theory", *Aerosp. Sci. Tech.*, **34**, 24-34.

CC